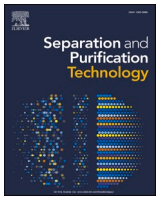
Separation and Purification Technology 413 (2026) 139722



Contents lists available at ScienceDirect

Separation and Purification Technology

journal homepage: www.elsevier.com/locate/seppur



Effect of solution conductivity on the anodic oxidation of diuron in secondary effluent

Izis C. Scutari [a], Carlos H.M. Fernandes [b], Renata Colombo [c], Diogo P. Volanti [a], Mauricio Boscolo [a], Marcos R.V. Lanza [b], Enric Brillas [d], Alexsandro J. dos Santos [a,*]

[a] Department of Chemistry and Environmental Sciences, São Paulo State University (UNESP), Rua Cristóvão Colombo 2265, São José do Rio Preto, SP 15054-000, Brazil
[b] São Carlos Institute of Chemistry, University of São Paulo, Avenida Trabalhador São-Carlense 400, São Carlos, SP 13566-590, Brazil
[c] School of Arts, Sciences and Humanities, University of São Paulo, Rua Arlindo Béttio 1000, 03828-000, São Paulo, SP, Brazil
[d] Departament de Ciència de Materials i Química Física, Facultat de Química, Universitat de Barcelona, Martí i Franquès 1-11, Barcelona, CP 08028, Spain

ARTICLE INFO

Editor name: Sergio Obregón

Keywords:
Anodic oxidation
Boron-doped diamond
Solution conductivity
Diuron
Secondary effluent
Hydroxyl radicals

ABSTRACT

Supporting electrolytes are commonly added in matrices in anodic oxidation (AO) electrolyses to increase the solution conductivity and reduce energy consumption, albeit this approach increases chemical demand and may not reflect real wastewater conditions. The present study investigated the feasibility and applicability of AO in the degradation of diuron, a model micropollutant, using a boron-doped diamond (BDD) anode under conductivity conditions representative of secondary effluents. The influence of current density, pH, diuron concentration, and solution conductivity was systematically evaluated. Reactive species were identified through scavenger experiments and electron paramagnetic resonance (EPR) analyses, and hydroxyl radicals were confirmed as the primary oxidizing species responsible for diuron degradation. Among the inorganic species investigated, chloride was found to enhance diuron degradation via the formation of reactive chlorine species, bicarbonate inhibited oxidation through radical scavenging, and nitrate and ammonium caused very minor effects. Complete diuron removal was achieved in a simulated secondary effluent with a solution conductivity of 1750 μS cm^{-1} absent adjustment. The influence of natural organic matter in diuron mineralization was thoroughly evaluated using humic acid, and dissolved organic carbon measurements indicated that the background organic matrix was only partially mineralized. In addition, 11 transformation products were identified and used to propose pathways for diuron degradation. ECOSAR predictions indicated that most transformation products exhibited lower predicted aquatic toxicity than the parent compound. Overall, the results demonstrate that AO is effective for diuron degradation in simulated secondary effluent under low-conductivity conditions without supplemental supporting electrolyte. These findings provide mechanistic insights and establish a basis for future validation using real secondary effluents.

1. Introduction

In recent years, large quantities of organic pollutants have been found to be indiscriminately released into the environment, which has contributed significantly to the widespread presence of micropollutants in aquatic systems [1,2]. These micropollutants include antibiotics, pesticides, dyes, and endocrine disruptors, many of which remain poorly understood in terms of their environmental occurrence and toxicity [2–6]. In response to this growing environmental concern, the European Union updated its urban wastewater treatment directive. The revised legislation establishes the implementation of advanced treatment technologies capable of ensuring the effective removal of a wide range of micropollutants by 2045 [7]. Despite such regulatory advances, similar challenges persist in countries such as Brazil, where intensive agricultural activities represent a major source of water contamination [8,9]. Herbicides such as diuron, widely used in sugarcane and citrus production, have been frequently detected in groundwater and drinking water, and this has raised serious environmental concerns worldwide [10–13]. Due to its persistence and limited biodegradability, diuron is not effectively removed by conventional wastewater treatment

* Corresponding author.
E-mail address: alexsandro.j.santos@unesp.br (A.J. dos Santos).

https://doi.org/10.1016/j.seppur.2026.139722
Received 28 June 2026; Received in revised form 6 August 2026; Accepted 11 August 2026
Available online 12 August 2026
1383-5866/© 2026 The Authors. Published by Elsevier B.V. This is an open access article under the CC BY license (http://creativecommons.org/licenses/by/4.0/).

processes. In an attempt to address this problem, there has been a dramatic spike in interest among researchers in the development of more efficient treatment technologies targeted at the monitoring of diuron in different matrices [14,15].

Among the emerging treatment technologies, anodic oxidation (AO) has attracted considerable attention as a versatile and scalable electrochemical approach for the treatment of chlorinated organic contaminants [16–18]. AO stands out for its operational simplicity and environmental compatibility. The process relies on the in situ generation of reactive species, using electrons as a clean reagent [19–21]. In this process, the anodic material plays a key role in determining the type and yield of oxidants formed. For non-active anodes such as boron-doped diamond (BDD), PbO_2, and Ti_4O_7, the electrogenerated hydroxyl radical ($^{\bullet}OH$)is widely recognized as the dominant oxidizing species due to its extremely high standard reduction potential (E° = 2.80 V). Consequently, $^{\bullet}OH$ is one of the most powerful oxidants in aqueous systems that allow the non-selective oxidation of a broad range of organic compounds [22–26]. In addition to the role played by the anodic material, the composition of the water matrix exerts a critical influence on AO performance by governing the formation and reactivity of electrogenerated oxidizing species. Previous studies have reported the generation of sulfate radicals and reactive chlorine species (Cl_2, HClO/ClO^-) during AO process, which can further enhance pollutant degradation [27–30]. This intrinsic flexibility makes AO particularly suitable for treating complex and variable water matrices, supporting its potential application in decentralized water treatment systems.

Despite these advantages, the practical implementation of AO is hindered by limitations related to electrolyte requirements. Although BDD AO has been extensively investigated for the degradation of diuron, most previous studies have primarily focused on maximizing degradation efficiency under lab conditions rather than assessing the practical applicability of the process. Consequently, most lab-scale studies rely on the addition of supporting electrolytes to increase solution conductivity. Although this improves current efficiency, it also increases operating costs and introduces additional chemicals into the treatment process [31–33]. Moreover, operating under artificially high conductivity conditions can lead to an overestimation of the performance of the treatment process, especially when evaluating energy consumption metrics such as electrical energy per order (EE/O). Interestingly, many real water matrices, including domestic wastewater and secondary effluents, already exhibit moderate conductivity levels, typically ranging from 950 to 3000 μS cm^{-1} [34–37]. Under these conditions, the addition of supporting electrolytes may not be required, although its impact on cell potential and overall energy consumption remains insufficiently understood. Thus, analyzing the efficiency of AO under realistic conductivity conditions is essential to provide a more accurate assessment of its performance and scalability. In this context, the design of electrochemical systems can move beyond generic optimization and instead consider the specific characteristics of the target water matrix. This enables more efficient, sustainable, and application-oriented treatment strategies.

Taking the aforementioned considerations into account, the present study investigates whether AO can remain effective under conductivity conditions representative of real secondary effluents, where ohmic limitations are expected to affect oxidant generation and energy consumption. Diuron was selected as a model pollutant for the analysis of degradation under low-conductivity conditions. The degradation study was performed by initially assessing the influence of key operating parameters, followed by the identification of the reactive species involved in the oxidation process. Particular attention was paid to the role of conductivity, considering not only its impact on degradation kinetics but also its implications for energy demand and the feasibility of the degradation process. The influence of inorganic ions, natural organic matter (NOM), and simulated secondary effluent was subsequently investigated to evaluate their impact on AO performance. Finally, transformation products derived from the degradation process were identified, and possible pathways for diuron degradation were proposed. By evaluating AO using the intrinsic conductivity of the water matrix, this work seeks to bridge the gap between lab mechanistic investigations and future validation using real secondary effluents.

2. Materials and methods

2.1. Chemicals and matrix preparation

Diuron (≥ 99%), sodium sulfate (Na_2SO_4, ≥ 99%), sodium chloride (NaCl, ≥ 99%), sodium nitrate ($NaNO_3$, ≥ 99%), humic acid (HA, technical grade), methanol (MeOH, ≥ 99.9%), tert-butanol (TBA, ≥ 99.5%), sodium persulfate ($Na_2S_2O_8$, ≥ 99%), and 5,5-dimethyl-1-pyrroline N-oxide (DMPO, ≥ 98%) were purchased from Sigma-Aldrich and used without further purification. Na_2SO_4 was used only when required to adjust conductivity in controlled experiments. Potassium iodide (KI, ≥ 97%) and sodium bicarbonate ($NaHCO_3$, ≥ 98%) were supplied by Êxodo Científica. NaCl, $NaHCO_3$, $NaNO_3$ and $(NH_4)_2SO_4$ were added to simulate common inorganic constituents (Cl^-, HCO_3^-/CO_3^{-2}, NO_3^-, and NH_4^+), whereas HA was used as a model of NOM. The solution pH was adjusted using diluted H_2SO_4 (98%) or NaOH. All solutions were prepared with ultrapure water (Milli-Q, 18.2 MΩ·cm) when required. A simulated secondary effluent (SE) was prepared to mimic the ionic composition of the real effluent [38]. The solution was composed of 336 mg L^{-1} $CaCO_3$, 244 mg L^{-1} NaCl, 110 mg L^{-1} $(NH_4)_2SO_4$, 87 mg L^{-1} $CaSO_4$, 32 mg L^{-1} $NaNO_3$, and 76 mg L^{-1} KCl, yielding a conductivity of ~1750 μS cm^{-1} and pH 7.0. To simulate the presence and variability of NOM, HA was added to achieve chemical oxygen demand (COD) levels ranging from 1 to 10 mg L^{-1}. Diuron was subsequently spiked into the synthetic matrix at a concentration of 1 mg L^{-1}. This approach allows one to evaluate the efficiency of the AO process under controlled, representative matrix conditions, accounting for variations in both organic load and contaminant presence.

2.2. Electrochemical procedure

AO assays were performed in a lab-scale undivided electrochemical reactor operating in batch mode with 100 mL of solution. The reactor was subjected to continuous magnetic stirring at 300 rpm to promote adequate mass transfer within the cell. Galvanostatic experiments were conducted using a DC power supply (Minipa MPS-3005B, 30 V, 5 A). BDD (NeoCoat) and stainless steel were employed as anode and cathode, respectively. The electrodes were positioned facing each other in parallel, separated by an interelectrode distance of 1 cm, with an effective geometric area of 3 cm^2. The effect of operating conditions was examined by varying the following parameters: initial diuron concentration (from 0.25 to 5.0 mg L^{-1}), applied current density (*j*) (from 4.0 to 32 mA cm^{-2}), and initial pH (from 3.0 to 10.0). The effects of inorganic ions, HA, and scavengers (MeOH and TBA) were also investigated.

Electrochemical characterization analysis was carried out by cyclic voltammetry (CV) and electrochemical impedance spectroscopy (EIS) using a Metrohm Autolab PGSTAT128N potentiostat/galvanostat equipped with a FRA32M module in a conventional three-electrode cell configuration which consisted of a BDD working electrode, an Ag/AgCl reference electrode (3 mol L^{-1} KCl), and a Pt counter electrode. CV measurements were recorded over a potential window of 0–3.0 V, at a scan rate of 25 mV s^{-1}. Based on the CV analysis, the onset of the oxygen evolution reaction was identified at approximately 2.3 V vs Ag/AgCl. EIS measurements were performed at this potential by applying a sinusoidal perturbation of 25 mV over a frequency range of 100 kHz to 10 mHz. Prior to each trial, the solution was purged with N_2 for 10 min to remove dissolved oxygen. Error bars shown in all figures correspond to the standard deviation of replicate measurements and were below 5%.

2.3. Analytical methods

Diuron concentrations were quantified using high-performance liquid chromatography (HPLC, Shimadzu LC-20AT) equipped with a C18 column (Phenomenex Luna, 250 × 4.6 mm, 5 μm) and a diode array detector (SPD-M20A). The mobile phase employed consisted of acetonitrile and water in the ratio of 70:30 *v*/v and was applied at a flow rate of 1.0 mL min^{-1}. Diuron was detected at λ = 250 nm and exhibited a retention time (RT) of 4.6 min. During electrolysis, aliquots were withdrawn at predetermined intervals, filtered through 0.45 μm membranes, and analyzed immediately. Persulfate (PS) was quantified spectrophotometrically via iodide oxidation, with absorbance measured at λ = 352 nm after 10 min of reaction. Hydrogen peroxide (H_2O_2) was determined using the Ti(IV) complexation method, which involved monitoring the peroxotitanium complex at λ = 408 nm [39].

Additional water quality parameters, including inorganic ions, free chlorine species, and COD, were determined using UV–Vis spectrophotometry (Hanna Instruments, IRIS model HI801–02) with commercial reagent kits, as per the manufacturer's instructions. Dissolved organic carbon (DOC) was measured using a total organic carbon analyzer (Shimadzu TOC-VCSN). Solution pH and electrical conductivity were measured using a multiparameter meter (Hanna Instruments, model HI6553P-02). Electron paramagnetic resonance (EPR) measurements were performed using DMPO (0.050 M) as a spin-trapping agent to analyze the formation of reactive species, including hydroxyl and sulfate radicals. Samples were collected after 3 min of electrolysis and analyzed using a Bruker ESR500 spectrometer. Spectra were recorded under standard operating conditions, with a sweep time of 60 s, modulation amplitude of 0.2 mT, and modulation frequency of 100 kHz.

Transformation products formed during diuron degradation were identified by liquid chromatography–tandem mass spectrometry (LC–MS/MS). The LC-MS/MS analyses were carried out using a Shimadzu LCMS-8030 triple quadrupole system equipped with an electrospray ionization (ESI) source. Separation was performed on a Shim-pack ODS II reversed-phase column (100 mm × 3.0 mm, 2.2 μm) with the temperature kept at 30 °C. The chromatographic system used ultrapure water containing 0.1% formic acid as solvent A and acetonitrile containing 0.1% formic acid as solvent B. A gradient elution program was applied, where the proportion of solvent B was increased from 10 to 37% during the first 5 min, followed by a ramping up to 100% B between 5 and 8 min. The initial conditions were restored from 8 to 10 min to allow the column to re-equilibrate. The flow rate was maintained at 0.5 mL min^{-1} throughout the analysis. Mass spectra were recorded in positive ESI mode. The ion source temperature was set at 400 °C and the interface voltage at 4.5 kV. Data were collected over a *m/z* interval of 50–500 in scan mode. Nitrogen was applied as both the nebulizing and drying gas at flow rates of 3 and 15 L min^{-1}, respectively.

2.4. Data processing methods

The efficiency of the AO process in diuron removal was calculated using Eq. (1):

$$\text{Removal efficiency } (\%) = \frac{c_0 - c}{c_0} \times 100 \quad (1)$$

where c_0 and c represent the initial and residual concentrations of diuron at electrolysis time *t*, respectively. The kinetics involving diuron degradation were evaluated assuming a pseudo-first-order kinetic model, which provided an excellent fit to the experimental data ($R^2 > 0.98$), as described in Eq. (2):

$$\ln\left(\frac{c_0}{c}\right) = k_1\, t \quad (2)$$

where the parameter k_1 is the apparent pseudo-first-order rate constant (min^{-1}). EE/O was used to evaluate the energy efficiency of the electrochemical process; this was determined using Eq. (3):

$$\text{EE}\Big/\text{O}\ \left(\text{kWh m}^{-3}\text{order}^{-1}\right) = \frac{E_{\text{cell}}\, I\, t}{V \log\left(\frac{c_0}{c}\right)} \quad (3)$$

where E_{cell} is the cell voltage (V), I is the applied current (A), V is the volume of the solution (L), and t is the electrolysis time (h). EE/O represents the electrical energy required to reduce the contaminant concentration by one order of magnitude (for >90% removal) per cubic meter of treated water.

The acute (LC50 and EC50) and chronic (ChV) aquatic toxicity of diuron and its transformation products was predicted using the Ecological Structure–Activity Relationships (ECOSAR) program. Predictions were generated for fish, daphnid, and green algae based on the molecular structures of the identified transformation products and used to provide a preliminary assessment of the predicted aquatic ecotoxicity of the identified transformation products.

To gain a thorough understanding of the contribution of reactive species in the electrochemical system, scavenging experiments were performed using varying concentrations of MeOH and TBA. The k_{MeOH} and k_{TBA} were determined as per Eq. (2), while the rate constant in the absence of scavengers was defined as $k_{control}$. The relative contributions of $^{\bullet}OH$ and sulfate radicals ($SO_4^{\bullet-}$) were estimated using Eqs. (4) and (5), respectively [40]:

$$\text{Contribution of } {}^{\bullet}\text{OH } (\%) = \frac{(k_{control} - k_{TBA})}{(k_{control})}\, 100 \quad (4)$$

$$\text{Contribution of } SO_4^{\bullet-} = \frac{(k_{TBA} - k_{MeOH})}{k_{control}} \quad (5)$$

3. Results and discussion

3.1. Influence of experimental variables

3.1.1. Effect of current density

The influence of *j* on diuron degradation in the AO process was initially evaluated at a fixed solution conductivity of 2000 μS cm^{-1}, as shown in Fig. 1a. A marked increase in *j* was found to accelerate the removal efficiency. After 180 min of electrolysis, 80% diuron removal was achieved at j = 4 mA cm^{-2}, which rose to 87% at j = 8 mA cm^{-2}. Near-complete degradation was achieved at j = 16 mA cm^{-2} after the same time (180 min), whereas at j = 32 mA cm^{-2}, total removal was obtained within only 40 min. An increase in *j* from 4 to 32 mA cm^{-2} resulted in an increase in k_1-value from 0.0091 to 0.109 min^{-1}, which corresponded to a roughly 12-fold increase in the degradation rate (see Table 1). This behavior is attributed to the enhanced generation of oxidizing species on the anode surface. When it comes to BDD anodes in AO processes, water oxidation leads to the formation of physisorbed hydroxyl radicals (BDD($^{\bullet}$OH)), which are weakly bound to the electrode surface and act as highly reactive oxidants toward diuron, as described in Eqs. (6) and (7) [41,42]. Hydroxyl radicals are known to react rapidly with aromatic pesticides, typically with second-order rate constants in the order of 10^9 M^{-1} s^{-1} [43]. An increase in *j* accelerated the electrogeneration of hydroxyl radicals on the BDD (BDD($^{\bullet}$OH)), leading to a faster diuron degradation.

$$\text{BDD} + H_2O \rightarrow \text{BDD}({}^{\bullet}\text{OH}) + H^+ + e^- \quad (6)$$

$$\text{BDD}({}^{\bullet}\text{OH}) + \text{Diuron} \rightarrow \text{by} - \text{products} \quad (7)$$

It should be noted however that the observed improvement in diuron degradation is accompanied by a marked increase in cell potential due to ohmic losses, which become particularly pronounced under low-conductivity conditions. This behavior is illustrated in Fig. 1b and reflects the intrinsic limitation imposed by the electrolyte resistance. In this perspective, an increase in *j* is constrained by the rapid rise in cell potential, which limits the practical operating window under these

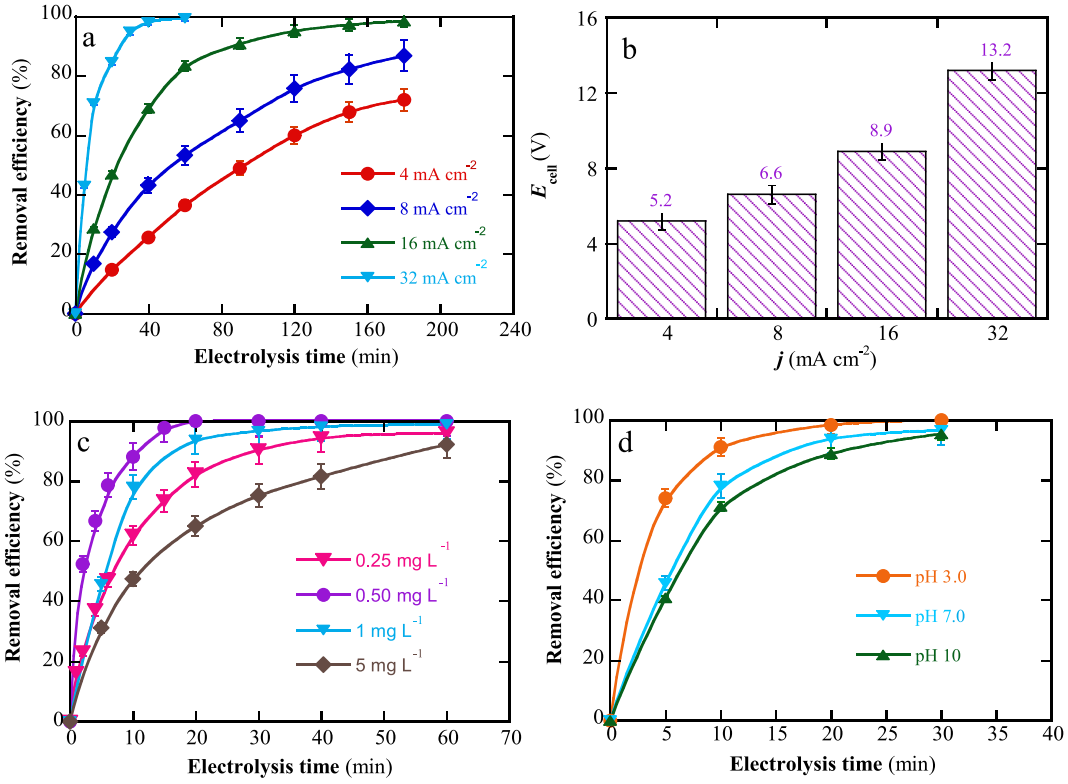


Fig. 1. Effect of current density on (a) percentage of diuron degradation vs. time and (b) cell voltage. (c) Initial diuron concentration and (d) pH applied in diuron degradation as a function of time. Experimental conditions: diuron = 1 mg L^{-1} (except in (c)), pH = 7.0 (except in (d)), conductivity = 2000 μS cm^{-1}, volume = 100 mL, and j = 32 mA cm^{-2} (except in (a) and (b)).

Table 1
Results obtained from the degradation of diuron under different experimental conditions.

Medium	Conductivity (μS cm^{-1})	[diuron] (mg L^{-1})	pH	j (mA cm^{-2})	% degradation (time)	k_1 (min^{-1})	R^2	EE/O (kWh m^{-3} $order^{-1}$)
Synthetic	2000	1.0	7.0	4	80 (180 min)	0.0091	0.999	–
Synthetic	2000	1.0	7.0	8	87 (180 min)	0.013	0.992	–
Synthetic	2000	1.0	7.0	16	99 (180 min)	0.045	0.994	6.78
Synthetic	2000	1.0	7.0	32	100 (40 min)	0.109	0.982	3.91
Synthetic	2000	0.25	7.0	32	95 (60 min)	0.077	0.988	6.28
Synthetic	2000	0.50	7.0	32	100 (20 min)	0.203	0.982	2.41
Synthetic	2000	5.0	7.0	32	92 (60 min)	0.044	0.991	11.0
Synthetic	2000	1.0	3.0	32	99 (20 min)	0.220	0.985	2.22
Synthetic	2000	1.0	10	32	99 (40 min)	0.101	0.996	5.10
Synthetic	930	1.0	7.0	32	96 (40 min)	0.055	0.991	13.1
Synthetic	9000	1.0	7.0	32	100 (10 min)	0.437	0.996	0.64
Synthetic	16,000	1.0	7.0	32	100 (6 min)	0.861	0.994	0.29
10 mM TBA	2000	1.0	7.0	32	31 (30 min)	0.0124	0.984	–
100 mM TBA	2000	1.0	7.0	32	25 (30 min)	0.0097	0.985	–
10 mM MeOH	2000	1.0	7.0	32	14 (30 min)	0.0043	0.992	–
100 mM MeOH	2000	1.0	7.0	32	10 (30 min)	0.0025	0.993	–
NO_3^-	2000	1.0	7.0	32	98 (30 min)	0.138	0.992	3.53
NH_4^+	2000	1.0	7.0	32	93 (30 min)	0.102	0.980	4.98
HCO_3^-	2000	1.0	7.0	32	94 (40 min)	0.067	0.998	7.31
Cl^-	2000	1.0	7.0	32	99 (10 min)	0.477	0.991	1.02
SE	9000	1.0	7.0	32	98 (40 min)	0.114	0.987	2.47
SE	1750	1.0	7.0	32	97 (40 min)	0.0728	0.993	7.20
SE + 1 mg L^{-1} HA	1750	1.0	7.0	32	96 (60 min)	0.0579	0.997	9.58
SE + 5 mg L^{-1} HA	1750	1.0	7.0	32	92 (60 min)	0.0442	0.996	11.8
SE + 10 mgL^{-1} HA	1750	1.0	7.0	32	83 (60 min)	0.0301	0.994	–

conditions. This observation points to a key underlying limitation of AO when applied in realistic water matrices, where conductivity directly restricts the applicable current density range.

3.1.2. *Effect of initial diuron concentration*

Fig. 1c shows the effect of initial diuron concentration applied in the range of 0.25–5 mg L^{-1}. As expected, higher diuron concentrations resulted in longer degradation periods, since more oxidizing species were required to achieve similar removal levels. At the highest

concentration of 5 mg L^{-1}, 92% removal was achieved after 60 min. In contrast, near-complete removal was obtained in shorter periods at the initial diuron concentrations of 0.5 and 1 mg L^{-1}. Interestingly, at the lowest diuron concentration of 0.25 mg L^{-1}, 95% removal was achieved only after approximately 60 min of treatment; this essentially points to a less efficient utilization of electrogenerated oxidizing species under the applied conditions.

The k_1 exhibited a non-linear dependence on the initial diuron concentration (see Table 1). Under the same galvanostatic conditions, the BDD($^{\bullet}OH$) generation rate remains constant, whereas the pollutant load is recorded at varying levels. As expected, higher concentrations lead to lower apparent reaction rates due to the greater demand for oxidizing species [44]. However, the decrease in k_1 at the lowest concentration suggests a less efficient utilization of electrogenerated oxidants.

In this regime, the reduced availability of pollutant molecules increases the likelihood of parallel non-oxidizing reactions consuming BDD($^{\bullet}OH$), like its dimerization to the weak oxidant H_2O_2, as per Eq. (8) [45]. As a result, a decrease is observed in the fraction of oxidants that effectively react with the target compound. This behavior reflects competition between diuron oxidation and other side reactions occurring in the system, rather than a limitation in the intrinsic oxidation capability [46].

$$2\ BDD(^{\bullet}OH) \rightarrow 2BDD + H_2O_2 \quad (8)$$

Overall, these results indicate that, under galvanostatic conditions, the efficiency of the AO process is governed by the balance between oxidant flux and pollutant load. This aspect becomes particularly relevant under low-conductivity conditions, where the generation of BDD ($^{\bullet}OH$) is inherently limited by the applied current, which directly impacts the process efficiency.

3.1.3. Effect of pH

The influence of the initial solution pH on diuron degradation was evaluated at pH 3.0, 7.0, and 10, the results of which are shown in Fig. 1d. The k_1-values obtained at the pH of 3.0, 7.0, and 10 were 0.220, 0.109, and 0.101 min^{-1}, respectively; this clearly indicates a noticeable improvement in degradation under acidic conditions, while similar efficiency was observed at neutral and alkaline pH (see also Table 1). This behavior can be explained by the pH dependence of the standard reduction potential of hydroxyl radicals. The redox potential of $^{\bullet}OH$ is approximately 2.80 V at pH 0 and decreases with increasing pH, reaching values close to ~2.1 V at pH 10 [47]. Consequently, the oxidizing strength of $^{\bullet}OH$ is higher under acidic conditions, which contributes to the observed kinetic enhancement at pH 3.0. Despite this thermodynamic effect, the small difference in k_1-value observed between pH 7.0 and 10 shows that the process is not strongly dependent on pH within this pH range. This suggests that the system efficiency is primarily governed by oxidant generation rather than variations in the reactivity of the radical species. From a practical standpoint, this behavior is particularly advantageous since it eliminates the need for pH adjustment, reduces the consumption of chemical reagents, and helps simplify the system operation. This operational situation is especially relevant to decentralized and point-of-use treatment systems, which are expected to operate under variable water-quality conditions without extensive chemical control.

3.2. Reactive species identification

For a comprehensive understanding of the reactive species involved in the process involving diuron degradation, scavenging experiments were performed using MeOH and TBA, which are widely used as radical quenchers. MeOH acts as a non-selective scavenger for both hydroxyl and sulfate radicals, whereas TBA is commonly used as a preferential scavenger for $^{\bullet}OH$ [48,49]. Electrolysis experiments were conducted for 30 min in the presence of increasing scavenger concentrations. As shown in Fig. 2a, the addition of 10 and 100 mM TBA significantly decreased the system efficiency in diuron removal from 94.2% to 31.4% and 25.2%, respectively, confirming the predominant role played by hydroxyl radicals in the process ($k_{TBA,\bullet OH} = 3.8 \times 10^8\ M^{-1}\ s^{-1}$). In contrast, the addition of MeOH resulted in a more pronounced inhibitory effect, reducing removal efficiencies to 14.5% and 9.2% at 10 and 100 mM, respectively. This higher reduction in the removal efficiency is attributed to the ability of MeOH to scavenge both $^{\bullet}OH$ ($k_{MeOH,\bullet OH} = 2.8 \times 10^9\ M^{-1}\ s^{-1}$) and $SO_4^{\bullet-}$ ($k_{MeOH,\ SO4\bullet}^{-} = 1.0 \times 10^7\ M^{-1}\ s^{-1}$), which essentially shows that $SO_4^{\bullet-}$ also contributes to the degradation process. The formation of $SO_4^{\bullet-}$ can be associated with the electrochemical oxidation of sulfate ions, as described in Eq. (9), followed by recombination to form PS, as described in Eq. (10) [50,51]:

$$SO_4^{2-} \rightarrow SO_4^{\cdot -} + e^- \quad (9)$$

$$2SO_4^{\cdot -} \rightarrow S_2O_8^{2-} \quad (10)$$

The removal efficiency of the system in the presence of scavengers followed pseudo-first-order kinetics, with k_1 values of 0.0097 min^{-1} and 0.0025 min^{-1} for TBA and MeOH, respectively. Based on Eqs. (4) and (5), the relative contributions of reactive species were estimated. Hydroxyl radical was identified as the dominant oxidizing species, accounting for approximately 90% of diuron degradation, followed by ~7% for sulfate radical. The remaining ~3% may be attributed to other reactive species not identified in this study (see the inset of Fig. 2a).

The contribution of direct electron transfer (DET) was evaluated by CV analyses. Fig. 2b shows that no oxidation peaks were observed prior to the onset of oxygen evolution in the presence of diuron; this shows that DET did not contribute significantly to the degradation process. Thus, the degradation process is mainly driven by electrogenerated reactive species. Regarding the formation of sulfate radical, two pathways can be considered. The first pathway occurs through Eqs. (9) and (10), leading to PS. The second pathway involves the direct cathodic reduction of PS to $SO_4^{\cdot -}$. In the present system, Fig. 2c shows that PS concentration increased continuously, reaching a maximum of approximately 80 mg L^{-1}, confirming its electrochemical generation. H_2O_2 was also detected at low concentrations (~1.24 mg L^{-1}), likely formed by recombination of hydroxyl radicals as per Eq. (8) [52]. Control experiments conducted in the absence of applied current, using only the electrogenerated persulfate and hydrogen peroxide, showed negligible diuron degradation; in essence, this shows that the radical species alone are insufficiently reactive unless further activation is promoted to generate $SO_4^{\bullet-}$ and $^{\bullet}OH$ [53].

EPR analysis using DMPO as a spin-trapping agent was performed in order to directly investigate the formation of radical species, as shown in Fig. 2d. As per the results obtained, no signal was observed at time zero; however, after 3 min of electrolysis, a clear quartet signal with an intensity ratio of 1:2:2:1 was detected in the 334–339 mT range, which is a typical characteristic of the DMPO–$^{\bullet}OH$ adduct [54]. This outcome provides direct evidence for the formation of $^{\bullet}OH$ under the applied conditions. In addition to the main quartet, small and less-resolved signals were also observed near the main peaks. These features do not follow the typical 1:2:2:1 pattern and are likely associated with other radical adducts, such as DMPO–$SO_4^{\cdot -}$. However, it is well known that DMPO– $SO_4^{\bullet-}$ is unstable in aqueous solution and can rapidly be converted into DMPO–$^{\bullet}OH$ [55]. In this sense, the EPR spectrum is dominated by the DMPO–$^{\bullet}OH$ signal, even when sulfate radicals are present. The combined evidence obtained from the scavenger experiments, electrochemical analysis, and EPR measurements consistently demonstrates that hydroxyl radicals are the primary oxidizing species in diuron degradation, and sulfate radicals also contribute but to a much lesser extent.

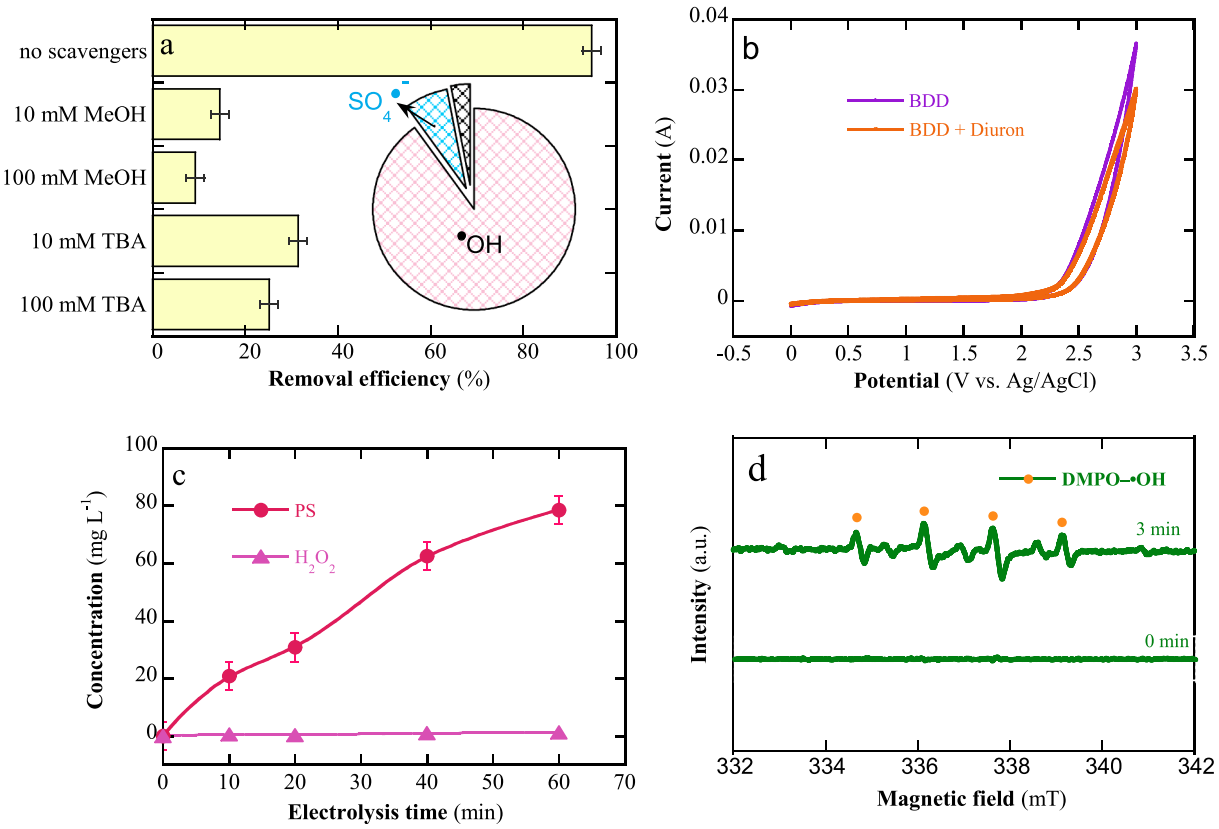


Fig. 2. (a) Effect of radical scavengers on diuron removal after 30 min of electrolysis; inset: relative contributions of •OH and $SO_4^{\bullet-}$. (b) CV in the presence and absence of diuron. (c) In situ formation of PS and H_2O_2. (d) EPR spectra recorded with DMPO during electrolysis in the absence of diuron.

3.3. Effect of solution conductivity on reaction kinetics and energy efficiency

Electrical conductivity plays a central role in electrochemical water treatment processes as it directly controls ohmic losses and, consequently, the effective utilization of the applied *j*. As shown in Fig. 3a, a marked increase in solution conductivity causes a drastic increase in diuron degradation. The results show that complete diuron removal was achieved within ~10 min of electrolysis at 9000 and 16,000 μS cm^{-1}, whereas under 930 μS cm^{-1}, one requires up to 60 min to obtain a similar removal efficiency. This pronounced difference in diuron removal indicates a transition from a kinetically controlled regime at high conductivity to an ohmic-limited regime at low conductivity [56].

The data related to the analysis of the dependence of kinetic and energy parameters on solution conductivity can be found in Fig. 3b and Table 1. As can be noted, an increase in conductivity leads to faster degradation rates with significant improvements in energy consumption efficiency. Considering that •OH has been identified as the dominant oxidizing species in sub-section 3.2, this behavior can be attributed to more effective AO conditions. Specifically, a decrease in ohmic losses minimizes a decrease in potential across the solution and increases the effective anodic potential, thereby promoting water oxidation on the electrode surface, as described in Eq. (6) [57]. Conversely, a decrease in solution conductivity leads to a substantial increase in energy demand (see Table 1). This shows that the system efficiency is progressively dominated by the solution resistance under low-conductivity conditions. In this regime, a significant fraction of the applied energy is dissipated as heat rather than contributing to electrochemical oxidation, severely compromising the process efficiency.

From an application perspective, although solution conductivities in the range of 9.0–16.0 mS cm^{-1} yield optimum electrochemical efficiency, achieving these conditions typically requires the addition of supporting electrolytes such as 7–14 g L^{-1} Na_2SO_4 [58]. However, this introduces two main drawbacks: (i) increased operating costs associated with the consumption of reagents; and (ii) the potential need for post-treatment to remove excess sulfate from the treated effluent. In contrast, moderate solution conductivity levels (2000 μS cm^{-1}) are representative of many real wastewater effluents and allow satisfactory degradation efficiency without additional electrolyte input. On the other hand, at very low solution conductivity, such as 930 μS cm^{-1}, the high energy demand observed makes electrochemical treatment economically unfavorable.

Additional mechanistic insights on diuron degradation under the AO process were obtained from electrochemical impedance spectroscopy analyses, as shown in Fig. 3c. Measurements performed at an anodic potential of +2.3 V vs Ag/AgCl revealed a clear decrease in solution resistance with increasing conductivity, as indicated by a reduction in the high-frequency intercept. In parallel, the decrease in semicircle diameter suggests enhanced charge transfer at the electrode –solution interface. These results confirm that solution conductivity not only mitigates ohmic limitations but also facilitates interfacial electrochemical processes.

Overall, these findings highlight a trade-off between energy efficiency and chemical reagent input. While high solution conductivity improves electrochemical performance, it often requires supporting electrolytes, increasing operating costs. Conversely, very low conductivity substantially increases energy demand. Therefore, solution conductivity emerges as one of the most influential operational parameters controlling the overall performance of the AO process.

3.4. Effect of coexisting inorganic substances

Inorganic ions commonly found in aquatic environments may interact with hydroxyl radicals and other electrogenerated oxidants,

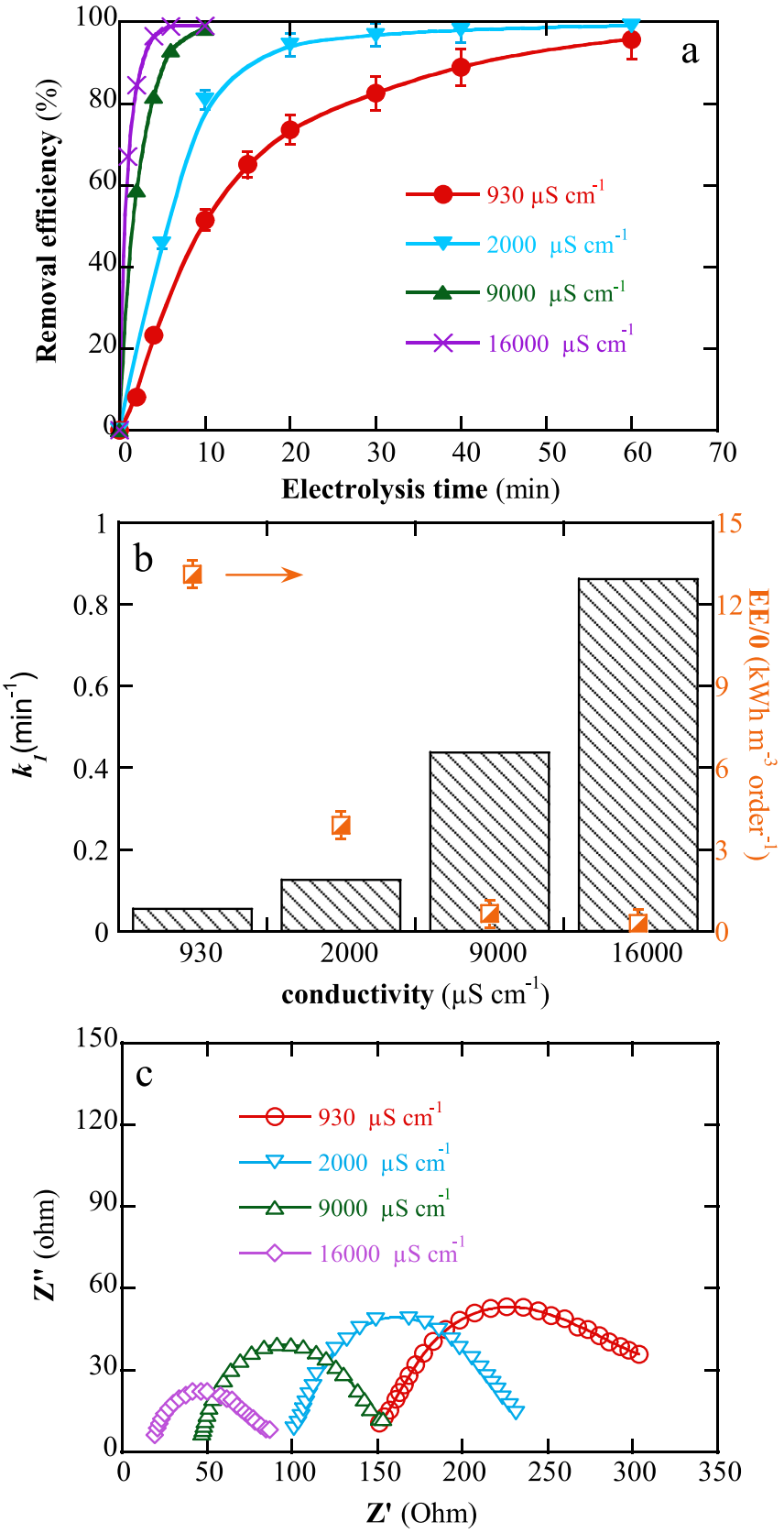


Fig. 3. Effect of conductivity on (a) diuron removal efficiency and (b) k_1 and EE/O. Electrolysis conditions: diuron = 1 mg L^{-1}, j = 32 mA cm^{-2}, pH = 7.0, and volume = 100 mL. (c) EIS at +2.3 V vs Ag/AgCl.

either inhibiting or promoting pollutant degradation. Taking this into account, the effects of Cl^-, NO_3^-, NH_4^+, and HCO_3^- in diuron degradation were evaluated under the following operating conditions: 2000 μS cm^{-1}, j = 32 mA cm^{-2}, and pH 7.0. As shown in Fig. 4a, the inorganic composition of the solution played an influential role in diuron degradation. The highest improvement in diuron degradation was recorded in the presence of Cl^-. Under these conditions, 90% diuron removal was achieved within 5 min, whereas almost complete degradation occurred after 10 min. As can be noted in Table 1, the k_1 value increased from 0.109 to 0.477 min^{-1}, corresponding to an approximately 4-fold enhancement relative to the control experiment result. At the same time, the EE/O decreased to 1.02 kWh m^{-3} $order^{-1}$. The rapid degradation observed in chloride-containing solutions is attributed to the electrogeneration of reactive chlorine species during electrolysis [59]. Cl^- is oxidized on the BDD surface to dissolved chlorine (Cl_2), which subsequently evolves into free chlorine species, such as HClO/ClO^-, depending on the solution pH [60]. Once generated, these oxidizing species diffuse into the bulk solution, where they contribute to indirect oxidation pathways and accelerate diuron degradation. Fig. 4b provides a clearer illustration of this phenomenon. During electrolysis, Cl^- concentration progressively decreased from 50 to approximately 23 mg L^{-1}, whereas free chlorine concentration continuously increased, reaching 3.2 mg L^{-1} at the end of the treatment. These findings confirm that the in situ formation of reactive free chlorine played an important role in the oxidation process.

NO_3^- and NH_4^+ exhibited very minor effects on diuron degradation. In the presence of NO_3^-, the k_1 value slightly increased from 0.109 to 0.138 min^{-1}, whereas the presence of NH_4^+ led to k_1 values very similar to those obtained in the control experiment (see Table 1). These results suggest that both species (NO_3^- and NH_4^+) behaved essentially as inert constituents under the conditions investigated. Although NO_3^- had limited influence on diuron oxidation, its behavior during electrolysis remains environmentally relevant because NO_3^- is one of the main inorganic contaminants in water [61]. The concentration profiles recorded from the electrolysis experiments revealed partial NO_3^- reduction accompanied by NO_2^- accumulation. As the electrolysis progressed, partial NO_2^- reoxidation was also observed, indicating the coexistence of reduction and oxidation pathways. At the end of the treatment, N-NO_3^- removal reached 14.8%, while N-NO_2^- concentration increased to 1.42 mg L^{-1}, with only trace N-NH_4^+ concentration (0.29 mg L^{-1}). In contrast, HCO_3^- negatively affected diuron degradation, where substantially longer electrolysis periods were required to achieve comparable removal efficiency. In the presence of bicarbonate, 95% diuron removal was only achieved after 60 min of electrolysis. This behavior is mainly attributed to the scavenging of hydroxyl radicals by HCO_3^- ($k = 8.5 \times 10^6$ M^{-1} s^{-1}), which decreases the availability of BDD ($^{\bullet}OH$) [62].

3.5. Efficiency of the AO-based system in a simulated secondary effluent

To assess the efficiency of the AO system under environmentally relevant conditions, experiments were conducted in a simulated secondary effluent containing representative inorganic constituents and NOM. As shown in Fig. 5a, complete diuron removal was achieved both in the simulated secondary effluent and in the same matrix after the solution conductivity was adjusted with Na_2SO_4. The addition of a supporting electrolyte increased conductivity from 1750 to approximately 9000 μS cm^{-1}, a range commonly used in AO analyses, resulting in faster degradation and improved energy efficiency. Under these conditions, the EE/O decreased from 7.20 to 2.47 kWh m^{-3} $order^{-1}$ (see Table 1). Nevertheless, the complete diuron removal obtained in the untreated matrix demonstrates that the intrinsic ionic content of secondary effluents can be sufficient to sustain effective AO without conductivity adjustment.

The influence of NOM, represented by HA in the simulated secondary effluent, was subsequently evaluated by varying its concentration from 0 to 10 mg L^{-1}, as presented in Fig. 5b. A progressive increase in HA concentration resulted in a decline in the kinetics of diuron degradation, with k_1 decreasing from 0.0728 to 0.0301 min^{-1} which corresponds to a 2.4-fold reduction. This behavior shows that NOM competes with the target pollutant for electrogenerated oxidants. Humic substances contain aromatic and oxygenated functional groups that readily react

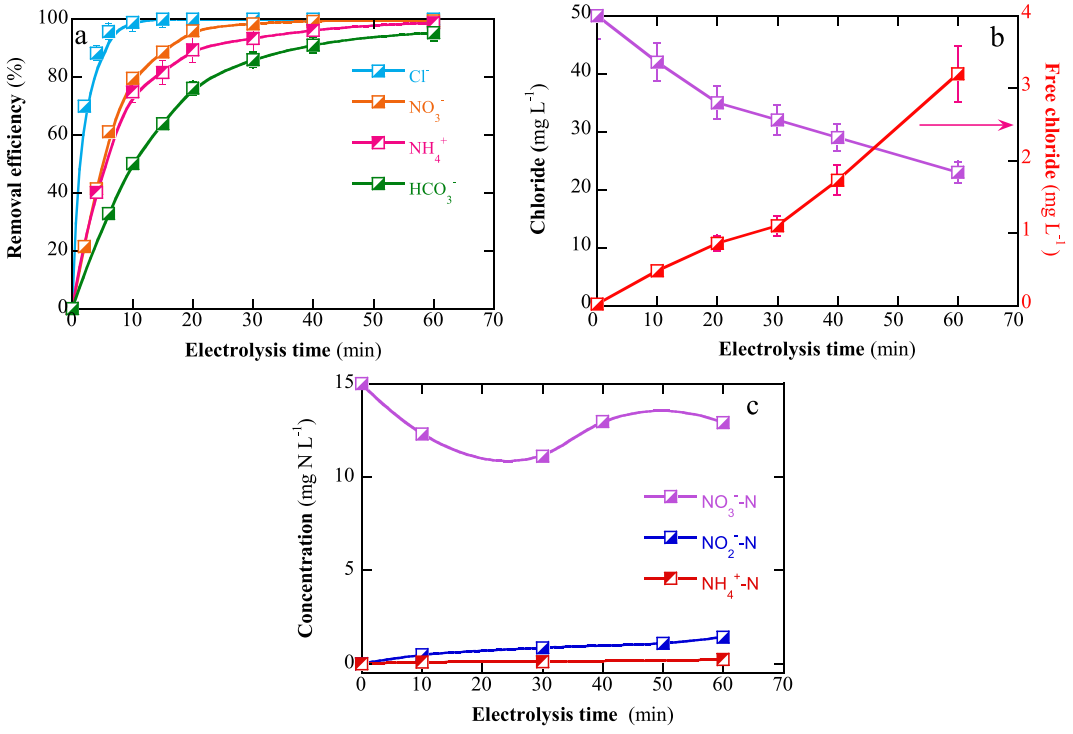


Fig. 4. (a) Effect of inorganic ions on diuron removal. (b) Decay of chloride and formation of active chlorine species during electrolysis in the presence of Cl^-. (c) Evolution of nitrogen species during nitrate electrolysis. Initial concentrations: Cl^- = 50 mg L^{-1}, NH_4^+/NO_3^- = 50 mg L^{-1}, HCO_3^- = 200 mg L^{-1}.

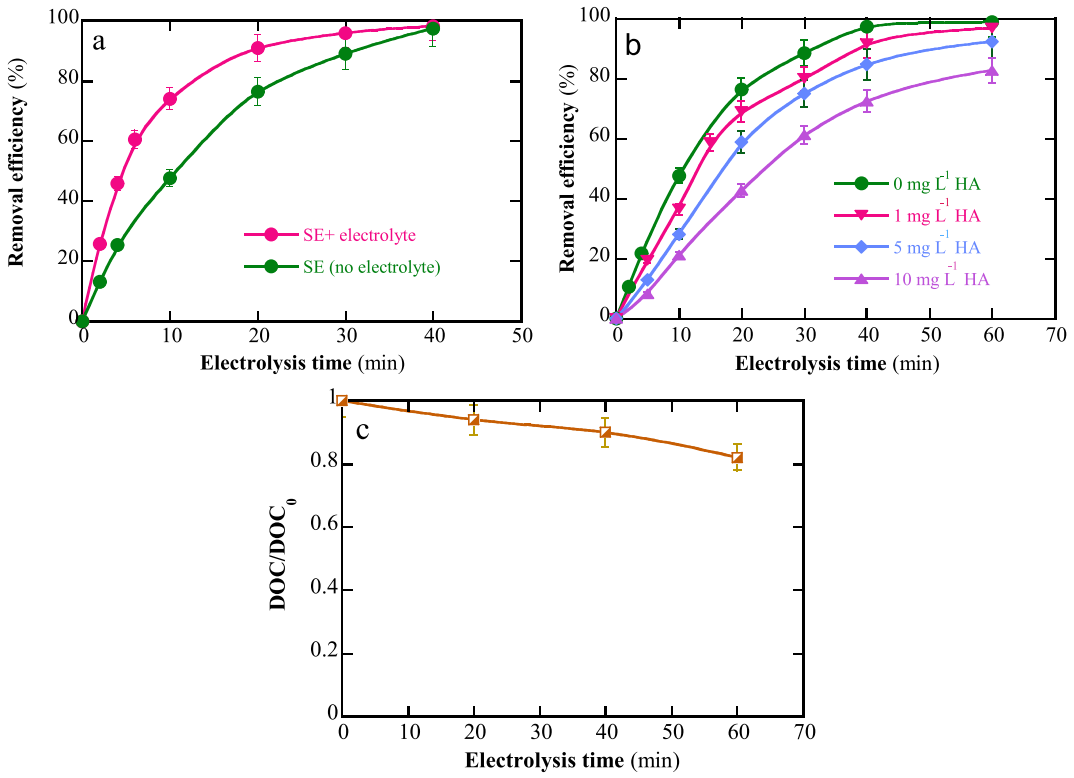
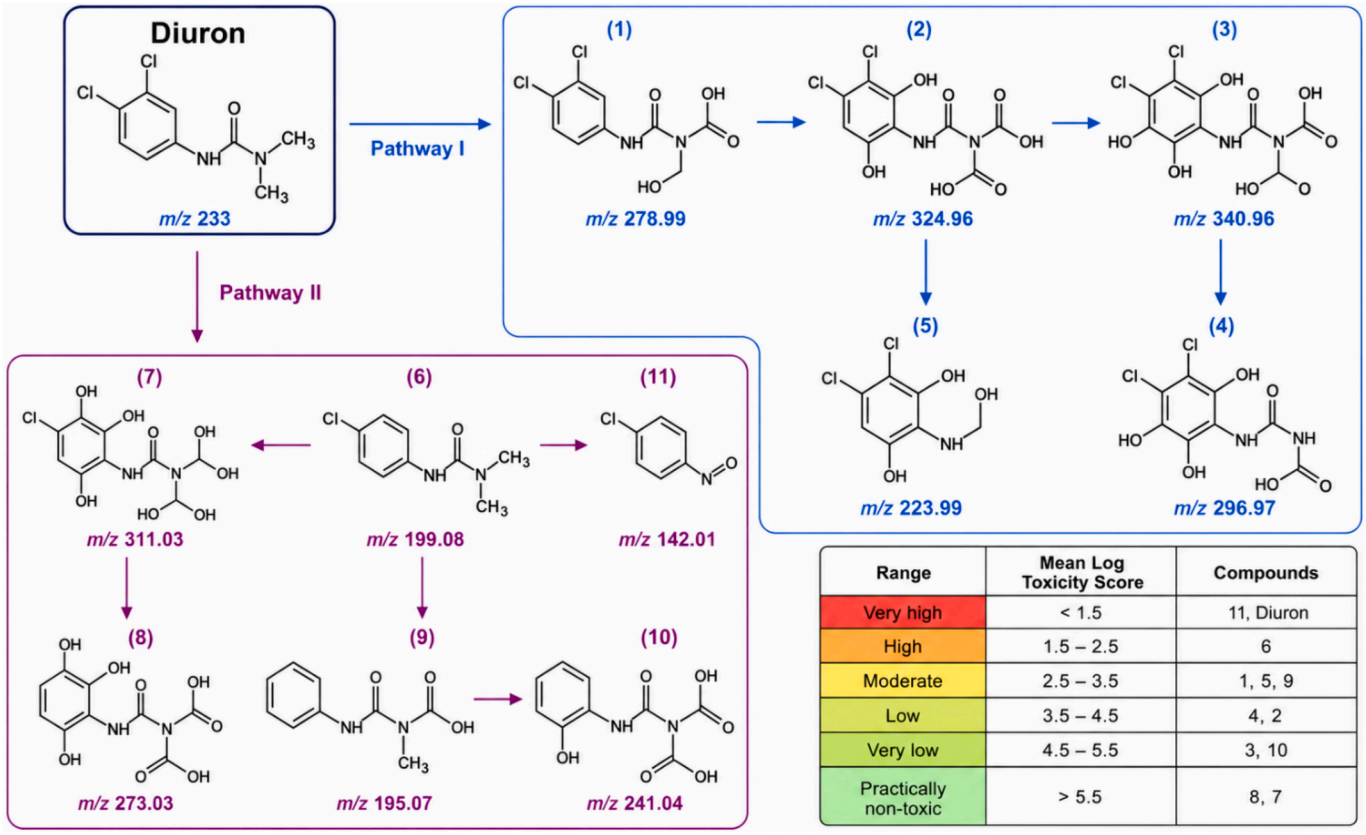


Fig. 5. (a) Comparative analysis of diuron degradation in a simulated secondary effluent of 1750 μS cm^{-1} and in the same matrix after adjusting the solution conductivity with Na_2SO_4 to approximately 9000 μS cm^{-1}. (b) Effect of HA on diuron degradation in the simulated secondary effluent. (c) DOC removal in the simulated secondary effluent in the presence of 10 mg L^{-1} HA.



Range	Mean Log Toxicity Score	Compounds
Very high	< 1.5	11, Diuron
High	1.5 – 2.5	6
Moderate	2.5 – 3.5	1, 5, 9
Low	3.5 – 4.5	4, 2
Very low	4.5 – 5.5	3, 10
Practically non-toxic	> 5.5	8, 7

Fig. 6. Proposed pathways for diuron degradation showing the main intermediates identified by LC–MS/MS and their predicted aquatic ecotoxicity. The color scale represents the relative toxicity categories predicted by ECOSAR.

with hydroxyl radicals and other oxidizing species, thereby reducing the fraction of reactive species available for diuron degradation [63].

The impact of NOM on diuron mineralization was assessed through DOC analyses performed in the simulated secondary effluent in the presence of 10 mg L^{-1} HA, the results of which can be found in Fig. 5c. After 60 min of electrolysis, DOC removal reached only 18%, indicating limited mineralization under the conditions investigated. It should be noted that the organic carbon content of the matrix was dominated by the added humic acid fraction rather than by diuron, whose contribution to the total carbon content was negligible. Thus, the modest DOC reduction observed mainly reflects the recalcitrant nature of humic substances and their oxidation products. More importantly, the low DOC removal recorded in the treatment process indicates that although the AO process remained effective in diuron degradation, substantially longer treatment periods would be required to achieve extensive mineralization.

3.6. Diuron degradation pathways and predicted ecotoxicity of transformation products

The degradation of diuron occurred through two major transformation pathways; these pathways involved successive hydroxylation, oxidation, dechlorination, and cleavage of the dimethylurea moiety, which gave rise to 11 transformation products, as shown in Fig. 6 and Table S1. Figs. S1 to S11 show the LC-MS fragments of the corresponding intermediates, and Fig. S12 presents the fragments recorded in the diuron removal process. The proposed mechanism in Fig. 6 shows that hydroxyl radical-mediated oxidation was the predominant degradation route during the electrolysis.

In Pathway 1, diuron ($m/z = 233.02$) initially undergoes oxidation of the dimethylurea side chain, yielding intermediate **1** ($m/z = 278.99$). Due to the high electrophilic character of $^{\bullet}OH$, hydrogen abstraction from the *N*-methyl groups is thermodynamically favorable, and this leads to the generation of carbon-centered radicals that rapidly react with dissolved oxygen and additional hydroxyl radicals [15,64,65]. Further oxidation gives rise to intermediate **2** ($m/z = 324.96$), which is indicative of the incorporation of additional oxygen into both the aromatic ring and the dimethylurea moiety. The phenylurea group increases electron density at the ortho and para positions of the aromatic ring through resonance effects, making these positions more susceptible to electrophilic attack by hydroxyl radicals [64–67].

The subsequent formation of intermediate **3** ($m/z = 340.96$), with an increase of 16 relative to intermediate **2**, is consistent with an additional hydroxylation reaction. The accumulation of oxygenated functionalities suggests extensive attack by reactive oxygen species, leading to highly oxidized structures. Intermediate **3** subsequently undergoes decarboxylation, producing compound **4** ($m/z = 296.97$), whereas cleavage and rearrangement of the oxidized urea side chain in intermediate **2** yield product **5** ($m/z = 223.99$).

Pathway 2 follows a different sequence dominated by dechlorination and progressive fragmentation reactions. In this route, diuron initially undergoes partial dechlorination and hydroxyl-radical-mediated attack on the aromatic ring, leading to the formation of monochlorinated intermediate **6** ($m/z = 199.08$). The loss of one chlorine atom and partial modification of the aromatic structure are consistent with radical substitution reactions that are commonly observed during electrochemical oxidation [15,68]. The cleavage of the C—Cl bond is facilitated by the electron-withdrawing nature of chlorine, which destabilizes the aromatic radical intermediates formed after attack by a hydroxyl radical.

Hydroxylation of intermediate **6** gives rise to oxygenated product **7** ($m/z = 311.03$). The mass increase of 112 points to the incorporation of multiple oxygen-containing functionalities through successive hydroxylation and oxidation reactions. Subsequent oxidative carboxylation and dechlorination of intermediate **7** lead to the formation of intermediate **8** ($m/z = 273.03$). Additional dechlorination and carboxylation reactions of intermediate **6** generate intermediate **9** ($m/z = 195.07$). Further oxidation and incorporation of oxygen-containing functionalities in intermediate **9** yield the terminal product **10** ($m/z = 241.04$). An alternative branch of Pathway 2 involves cleavage of the aryl–urea bond, which gives rise to aromatic intermediate **11** ($m/z = 142.01$) [69].

Although quantitative determination of the transformation products was not performed due to the lack of analytical standards, their temporal evolution during electrolysis was evaluated semi-quantitatively based on the relative LC-MS signal intensities obtained at different treatment times (0–60 min). Four transformation products (2, 4, 7, and 10) were detected within the first 10 min of electrolysis and remained present until the end of the treatment, showing comparable relative signal intensities over time, which suggests that these compounds are the most persistent intermediates under the investigated conditions. In contrast, the remaining transformation products were transient species, appearing mainly during intermediate stages of electrolysis (20–50 min) with distinct temporal profiles before disappearing from the chromatograms. This behavior indicates a dynamic transformation process in which most intermediates are further degraded as electrolysis progresses, while only a limited number of relatively stable products persist after complete removal of the parent compound.

To provide a preliminary environmental assessment of the identified transformation products, their aquatic ecotoxicity was predicted using the ECOSAR model. As shown in Fig. 6 and Table S2, most hydroxylated and carboxylated intermediates exhibited substantially lower predicted acute and chronic aquatic toxicity than diuron, particularly compounds 7 and 8. Although one transformation product (compound 11) presented toxicity values comparable to those of the parent compound, its environmental relevance cannot be inferred solely from ECOSAR predictions because its actual concentration, persistence, and formation yield were not determined.

Notably, the transformation products that persisted after 60 min of electrolysis (compounds 2, 4, 7, and 10) were classified by ECOSAR as having low to negligible predicted toxicity. This observation suggests a shift toward less toxic species during the treatment process. However, this interpretation should be considered preliminary, as it is based on predictive modeling and relative signal intensities rather than experimentally validated ecotoxicological data or quantitative concentration profiles.

Overall, the results indicate that the predominant oxidation pathway leads to the formation of transformation products with lower predicted aquatic toxicity than diuron; however, conclusions regarding environmental safety should be interpreted with caution and limited to a preliminary assessment under the specific experimental conditions investigated.

4. Conclusions

This study demonstrated that AO using a BDD anode is an effective strategy for the degradation of diuron in simulated secondary effluent at environmentally relevant conductivity levels, without the need for supporting electrolyte addition. Solution conductivity was identified as a key operational parameter governing both degradation kinetics and energy consumption, while hydroxyl radicals were confirmed as the predominant oxidizing species responsible for diuron degradation. Furthermore, the effects of inorganic ions and NOM were systematically evaluated, 11 transformation products were identified, and ECOSAR predictions indicated that most transformation products exhibited lower predicted aquatic toxicity than the parent compound. Simulated secondary effluent was intentionally selected to provide a controlled experimental matrix for systematically investigating the effects of solution conductivity, reactive species, and water constituents on AO performance. Such mechanistic studies are an essential step toward understanding and optimizing electrochemical treatment processes before validation using real secondary effluents, whose physicochemical characteristics vary among wastewater treatment plants and geographical regions and may substantially influence process performance. These

findings establish the mechanistic and operational basis for this next stage of development. Future studies should validate the proposed process using real secondary effluents, experimentally assess the toxicity of treated samples and transformation products, perform techno-economic analyses, and evaluate process scale-up to support future technology transfer.

CRediT authorship contribution statement

Izis C. Scutari: Writing – review & editing, Visualization, Formal analysis, Data curation. **Carlos H.M. Fernandes:** Writing – review & editing, Data curation. **Renata Colombo:** Writing – review & editing, Data curation. **Diogo P. Volanti:** Writing – review & editing, Methodology. **Mauricio Boscolo:** Writing – review & editing, Validation. **Marcos R.V. Lanza:** Writing – review & editing, Methodology. **Enric Brillas:** Writing – review & editing, Validation, Methodology. **Alexsandro J. dos Santos:** Writing – review & editing, Writing – original draft, Supervision, Project administration, Conceptualization.

Declaration of competing interest

The authors declare that they have no known competing financial interests or personal relationships that could have appeared to influence the work reported in this paper.

Acknowledgments

This study was funded, in part, by the São Paulo Research Foundation (FAPESP), Brazil (Process numbers #2020/06421-1, #2022/12895-1, #2023/06558-5, #2023/16167-3, #2024/06046-7, #2024/13890-9, #2025/05801-9, #2025/16092-9) and the Brazilian National Council for Scientific and Technological Development – CNPq (Brazil) (grant #303943/2021-1, 305542/2024-9 and #401122/2025-5).

Appendix A. Supplementary data

Supplementary data to this article can be found online at https://doi.org/10.1016/j.seppur.2026.139722.

Data availability

Data will be made available on request.

References

[1] C. Simarro-Gimeno, M. Otoukesh, E.A. Serna Galvis, R.A. Torres-Palma, E. Pitarch, F. Hernández, Investigation of organic micropollutants in urban wastewater and the feasibility of reusing treated wastewater for irrigation purposes, J. Environ. Chem. Eng. 13 (2025) 116216, https://doi.org/10.1016/j.jece.2025.116216.

[2] Y. Luo, W. Guo, H.H. Ngo, L.D. Nghiem, F.I. Hai, J. Zhang, S. Liang, X.C. Wang, A review on the occurrence of micropollutants in the aquatic environment and their fate and removal during wastewater treatment, Sci. Total Environ. 473–474 (2014) 619–641, https://doi.org/10.1016/j.scitotenv.2013.12.065.

[3] J. Rogowska, M. Cieszynska-Semenowicz, W. Ratajczyk, L. Wolska, Micropollutants in treated wastewater, Ambio 49 (2020) 487–503, https://doi.org/10.1007/s13280-019-01219-5.

[4] Z. Tian, H. Zhao, K.T. Peter, M. Gonzalez, J. Wetzel, C. Wu, X. Hu, J. Prat, E. Mudrock, R. Hettinger, A.E. Cortina, R.G. Biswas, F.V.C. Kock, R. Soong, A. Jenne, B. Du, F. Hou, H. He, R. Lundeen, A. Gilbreath, R. Sutton, N.L. Scholz, J. W. Davis, M.C. Dodd, A. Simpson, J.K. McIntyre, E.P. Kolodziej, A ubiquitous tire rubber–derived chemical induces acute mortality in coho salmon, Science 371 (2021) 185–189, https://doi.org/10.1126/science.abd6951.

[5] G. Ersan, A.J. dos Santos, M.R.V. Lanza, F. Perreault, S. Garcia-Segura, Enhancing the selective ciprofloxacin adsorption in urine matrices through the metal-doping of carbon sorbents, J. Environ. Manag. 348 (2023) 119298, https://doi.org/10.1016/j.jenvman.2023.119298.

[6] J. Yang, L. Huang, J. You, Y. Yamauchi, Magnetic covalent organic framework composites for wastewater remediation, Small 19 (2023), https://doi.org/10.1002/smll.202301044.

[7] X. Cui, C. Peng, W. Duan, Y. Lian, Y. Chen, T. Guan, T. Kong, R. Wan, J. Chen, J.-J. Chen, Z. Tang, H.-Q. Yu, Y. Xiong, Scalable flow-through device for electrochemical water treatment without secondary pollution, Nat. Sustainability (2026), https://doi.org/10.1038/s41893-026-01799-7.

[8] L.O. Cossu, S.F. De Aquino, C.R. Mota Filho, C.J. Smith, M. Vignola, Review on pesticide contamination and drinking water treatment in Brazil: the need for improved treatment methods, ACS ES&T Water 4 (2024) 3629–3644, https://doi.org/10.1021/acsestwater.4c00063.

[9] A.J.M. da Costa, M.S. Kronka, P.J.M. Cordeiro-Junior, G.V. Fortunato, A.J. dos Santos, M.R.V. Lanza, Treatment of tebuthiuron in synthetic and real wastewater using electrochemical flow-by reactor, J. Electroanal. Chem. 882 (2021) 114978, https://doi.org/10.1016/j.jelechem.2021.114978.

[10] E.F.G.C. Dores, C.A. Spadotto, O.L.S. Weber, L. Carbo, A.B. Vecchiato, A.A. Pinto, Environmental behaviour of metolachlor and diuron in a tropical soil in the central region of Brazil, Water Air Soil Pollut. 197 (2009) 175–183, https://doi.org/10.1007/s11270-008-9801-1.

[11] A.C. da Silva, T.S. da Sena, I.G.S. Oliveira, F.E. Bimbi Junior, O.C. Junior, R. S. Souto, M.M. Baruch, J.P.P. Encide, K.M. Honorio, M.R.V. Lanza, A.E. de Carvalho, W.R.P. Barros, Electrochemical determination of diuron in Brazilian crops: f-MWCNT@chi-AgNPs nanocomposite-modified screen-printed electrode for food safety monitoring, FlatChem 54 (2025) 100929, https://doi.org/10.1016/j.flatc.2025.100929.

[12] C. Panis, L.Z.P. Candiotto, S.C. Gaboardi, S. Gurzenda, J. Cruz, M. Castro, B. Lemos, Widespread pesticide contamination of drinking water and impact on cancer risk in Brazil, Environ. Int. 165 (2022) 107321, https://doi.org/10.1016/j.envint.2022.107321.

[13] R. Loos, G. Locoro, S. Comero, S. Contini, D. Schwesig, F. Werres, P. Balsaa, O. Gans, S. Weiss, L. Blaha, M. Bolchi, B.M. Gawlik, Pan-european survey on the occurrence of selected polar organic persistent pollutants in ground water, Water Res. 44 (2010) 4115–4126, https://doi.org/10.1016/j.watres.2010.05.032.

[14] C. Jayasumana, P. Paranagama, S. Agampodi, C. Wijewardane, S. Gunatilake, S. Siribaddana, Drinking well water and occupational exposure to herbicides is associated with chronic kidney disease, in Padavi-Sripura, Sri Lanka, Environ. Health 14 (2015) 6, https://doi.org/10.1186/1476-069X-14-6.

[15] S. Giacomazzi, N. Cochet, Environmental impact of diuron transformation: a review, Chemosphere 56 (2004) 1021–1032, https://doi.org/10.1016/j.chemosphere.2004.04.061.

[16] R.F. Gutiérrez-Hernández, R. Bello-Mendoza, A. Hernández-Ramírez, E.A. Malo, H. A. Nájera-Aguilar, Photo-assisted electrochemical degradation of polychlorinated biphenyls with boron-doped diamond electrodes, Environ. Technol. 40 (2019) 2718–2730, https://doi.org/10.1080/09593330.2017.1375999.

[17] P. Cañizares, J. García-Gómez, C. Sáez, M.A. Rodrigo, Electrochemical oxidation of several chlorophenols on diamond electrodes. Part I. Reaction mechanism, J. Appl. Electrochem. 33 (2003) 917–927, https://doi.org/10.1023/A:1025888126686.

[18] M. Herraiz-Carboné, A. Santos, A. Hayat, C.M. Domínguez, S. Cotillas, Remediation of groundwater polluted with lindane production wastes by conductive-diamond electrochemical oxidation, Sci. Total Environ. 926 (2024) 171848, https://doi.org/10.1016/j.scitotenv.2024.171848.

[19] A.J. dos Santos, E. Brillas, A review of anodic oxidation, electro-Fenton and electrochemical nitrate reduction: a decade of advances and future directions, J. Electroanal. Chem. 1009 (2026) 119996, https://doi.org/10.1016/j.jelechem.2026.119996.

[20] B.P. Chaplin, The prospect of electrochemical technologies advancing worldwide water treatment, Acc. Chem. Res. 52 (2019) 596–604, https://doi.org/10.1021/acs.accounts.8b00611.

[21] Z. Chen, X. Wang, H. Feng, S. Chen, J. Niu, G. Di, D. Kujawski, J.C. Crittenden, Electrochemical advanced oxidation of perfluorooctanoic acid: mechanisms and process optimization with kinetic modeling, Environ. Sci. Technol. 56 (2022) 14409–14417, https://doi.org/10.1021/acs.est.2c02906.

[22] Z. Hu, J. Cai, G. Song, Y. Tian, M. Zhou, Anodic oxidation of organic pollutants: anode fabrication, process hybrid and environmental applications, Curr. Opin. Electrochem. 26 (2021) 100659, https://doi.org/10.1016/j.coelec.2020.100659.

[23] J. Teng, Y. Zhang, P. Li, G. Liu, Hydroxyl radical in anodic oxidation-based electrochemical advanced oxidation processes: critical understanding and a new perspective, Sustainable Horiz. 16 (2025) 100156, https://doi.org/10.1016/j.horiz.2025.100156.

[24] J. Wang, D. Zhi, H. Zhou, X. He, D. Zhang, Evaluating tetracycline degradation pathway and intermediate toxicity during the electrochemical oxidation over a Ti/Ti_4O_7 anode, Water Res. 137 (2018) 324–334, https://doi.org/10.1016/j.watres.2018.03.030.

[25] C. Wang, T. Zhang, J. Luo, M. Wu, J. Niu, E. Shang, C. Ni, J. Ni, Synergistic enhancement of piezocatalysis and electrochemical oxidation for the degradation of ciprofloxacin by PbO_2 intercalation material, Sep. Purif. Technol. 297 (2022) 121528, https://doi.org/10.1016/j.seppur.2022.121528.

[26] S.O. Ganiyu, N. Oturan, S. Raffy, M. Cretin, R. Esmilaire, E. van Hullebusch, G. Esposito, M.A. Oturan, Sub-stoichiometric titanium oxide (Ti_4O_7) as a suitable ceramic anode for electrooxidation of organic pollutants: a case study of kinetics, mineralization and toxicity assessment of amoxicillin, Water Res. 106 (2016) 171–182, https://doi.org/10.1016/j.watres.2016.09.056.

[27] P. Chanikya, P.V. Nidheesh, D. Syam Babu, A. Gopinath, M. Suresh Kumar, Treatment of dyeing wastewater by combined sulfate radical based electrochemical advanced oxidation and electrocoagulation processes, Sep. Purif. Technol. 254 (2021) 117570, https://doi.org/10.1016/j.seppur.2020.117570.

[28] I. Sánchez-Montes, G.O.S. Santos, A.J. dos Santos, C.H.M. Fernandes, R.S. Souto, P. Chelme-Ayala, M.G. El-Din, M.R.V. Lanza, Toxicological aspect of water treated by chlorine-based advanced oxidation processes: a review, Sci. Total Environ. 878 (2023) 163047, https://doi.org/10.1016/j.scitotenv.2023.163047.

[29] E. del Rosario Salas-Sandoval, T. Pérez-Segura, S. Garcia-Segura, A.J. dos Santos, Innovative approaches to electrochemical oxidation of bisphenol B in synthetic and complex water environments, Sci. Total Environ. 955 (2024) 176762, https://doi.org/10.1016/j.scitotenv.2024.176762.
[30] S. Cotillas, E. Lacasa, C. Sáez, P. Cañizares, M.A. Rodrigo, Disinfection of urine by conductive-diamond electrochemical oxidation, Appl. Catal. B Environ. 229 (2018) 63–70, https://doi.org/10.1016/j.apcatb.2018.02.013.
[31] J. Chen, S. Zhong, X. Duan, Electrifying water treatment at device level, Nat. Sustainability (2026), https://doi.org/10.1038/s41893-026-01806-x.
[32] D. Clematis, M. Panizza, Electrochemical oxidation of organic pollutants in low conductive solutions, Curr. Opin. Electrochem. 26 (2021) 100665, https://doi.org/10.1016/j.coelec.2020.100665.
[33] S. Garcia-Segura, J.D. Ocon, M.N. Chong, Electrochemical oxidation remediation of real wastewater effluents — a review, Process. Saf. Environ. Prot. 113 (2018) 48–67, https://doi.org/10.1016/j.psep.2017.09.014.
[34] Z. Bogart, A. Atrashkevich, J. Ananpattarachai, S. Sinha, S. Garcia-Segura, P. Westerhoff, Towards low energy greywater treatment of surfactants and pathogens, Discov. Water 5 (2025) 96, https://doi.org/10.1007/s43832-025-00295-x.
[35] H.L. Barazorda-Ccahuana, A.S. Fajardo, A.J. dos Santos, M.R.V. Lanza, Decentralized approach toward organic pollutants removal using UV radiation in combination with H_2O_2-based electrochemical water technologies, Chemosphere 342 (2023) 140079, https://doi.org/10.1016/j.chemosphere.2023.140079.
[36] S. Garcia-Segura, J. Keller, E. Brillas, J. Radjenovic, Removal of organic contaminants from secondary effluent by anodic oxidation with a boron-doped diamond anode as tertiary treatment, J. Hazard. Mater. 283 (2015) 551–557, https://doi.org/10.1016/j.jhazmat.2014.10.003.
[37] R. Liang, S. Li, X. Zhang, Z. Hu, H. Wu, J. Sun, G. Song, J. Liu, Y. Chai, I. Sirés, M. Zhou, Highly efficient singlet oxygen production in a cascade photoelectrocatalytic system for water decontamination, Angew. Chem. Int. Ed. 64 (2025), https://doi.org/10.1002/anie.202508548.
[38] O. El Kik, F. Zaviska, G. Lesage, A. Sauvêtre, F. Lestremau, M. Heran, Optimizing electro-oxidation for selective trace micropollutant removal and energy efficiency in secondary effluents, Water Res. 291 (2026) 125158, https://doi.org/10.1016/j.watres.2025.125158.
[39] C. Matsubara, N. Kawamoto, K. Takamura, Oxo[5, 10, 15, 20-tetra(4-pyridyl)porphyrinato]titanium(IV): an ultra-high sensitivity spectrophotometric reagent for hydrogen peroxide, Analyst 117 (1992) 1781, https://doi.org/10.1039/an9921701781.
[40] S. Yang, Y. Feng, D. Gao, X. Wang, N. Suo, Y. Yu, S. Zhang, Electrocatalysis degradation of tetracycline in a three-dimensional aeration electrocatalysis reactor (3D-AER) with a flotation-tailings particle electrode (FPE): physicochemical properties, influencing factors and the degradation mechanism, J. Hazard. Mater. 407 (2021) 124361, https://doi.org/10.1016/j.jhazmat.2020.124361.
[41] M. Panizza, G. Cerisola, Direct and mediated anodic oxidation of organic pollutants, Chem. Rev. 109 (2009) 6541–6569, https://doi.org/10.1021/cr9001319.
[42] A.J. dos Santos, H. Shen, M.R.V. Lanza, Q. Li, S. Garcia-Segura, Electrochemical oxidation of surfactants as an essential step to enable greywater reuse, Environ. Technol. Innov. 34 (2024) 103563, https://doi.org/10.1016/j.eti.2024.103563.
[43] G.V. Buxton, C.L. Greenstock, W.P. Helman, A.B. Ross, Critical review of rate constants for reactions of hydrated electrons, hydrogen atoms and hydroxyl radicals (OH/O) – in aqueous solution, J. Phys. Chem. Ref. Data Monogr. 17 (1988) 513–886, https://doi.org/10.1063/1.555805.
[44] B. Marselli, J. Garcia-Gomez, P.-A. Michaud, M.A. Rodrigo, Ch. Comninellis, Electrogeneration of hydroxyl radicals on boron-doped diamond electrodes, J. Electrochem. Soc. 150 (2003) D79, https://doi.org/10.1149/1.1553790.
[45] A. Kapałka, G. Fóti, C. Comninellis, The importance of electrode material in environmental electrochemistry, Electrochim. Acta 54 (2009) 2018–2023, https://doi.org/10.1016/j.electacta.2008.06.045.
[46] S. Garcia-Segura, A.B. Nienhauser, A.S. Fajardo, R. Bansal, C.L. Conrad, J. D. Fortner, M. Marcos-Hernández, T. Rogers, D. Villagran, M.S. Wong, P. Westerhoff, Disparities between experimental and environmental conditions: research steps toward making electrochemical water treatment a reality, Curr. Opin. Electrochem. 22 (2020) 9–16, https://doi.org/10.1016/j.coelec.2020.03.001.
[47] U. Hübner, S. Spahr, H. Lutze, A. Wieland, S. Rüting, W. Gernjak, J. Wenk, Advanced oxidation processes for water and wastewater treatment – guidance for systematic future research, Heliyon 10 (2024) e30402, https://doi.org/10.1016/j.heliyon.2024.e30402.
[48] W. Li, G. Song, J. Jing, X. Ren, C. Zhang, M.A. Oturan, M. Zhou, Identification and quantification of reactive species in aqueous medium during application of advanced oxidation processes: a critical review, Chem. Eng. J. 500 (2024) 156698, https://doi.org/10.1016/j.cej.2024.156698.
[49] G.A. Cerrón-Calle, M. Flores, M.A. Roldan, K. Flores, E. Brillas, A.J. dos Santos, S. Garcia-Segura, Electrochemical persulfate activation for degradation of BPA using a novel self-standing CuOx/CoOx cathode, Chem. Eng. J. 519 (2025) 164960, https://doi.org/10.1016/j.cej.2025.164960.
[50] H. Song, L. Yan, J. Jiang, J. Ma, Z. Zhang, J. Zhang, P. Liu, T. Yang, Electrochemical activation of persulfates at BDD anode: radical or nonradical oxidation? Water Res. 128 (2018) 393–401, https://doi.org/10.1016/j.watres.2017.10.018.
[51] G. Ren, J. Zhang, X. Wang, G. Liu, M. Zhou, A critical review of persulfate-based electrochemical advanced oxidation processes for the degradation of emerging contaminants: from mechanisms and electrode materials to applications, Sci. Total Environ. 944 (2024) 173839, https://doi.org/10.1016/j.scitotenv.2024.173839.
[52] P.J. Espinoza-Montero, P. Alulema-Pullupaxi, B.A. Frontana-Uribe, C.E. Barrera-Diaz, Electrochemical production of hydrogen peroxide on boron-doped diamond (BDD) electrode, Curr. Opin. Solid State Mater. Sci. 26 (2022) 100988, https://doi.org/10.1016/j.cossms.2022.100988.
[53] M.S. Gaber, S. Garcia-Segura, M.R.V. Lanza, A.J. dos Santos, Enabling decentralized treatment of BPA through electrified photo-activated advanced oxidation, Sep. Purif. Technol. 382 (2026) 136095, https://doi.org/10.1016/j.seppur.2025.136095.
[54] J. Cai, T. Niu, P. Shi, G. Zhao, Boron-doped diamond for hydroxyl radical and sulfate radical anion electrogeneration, transformation, and voltage-free sustainable oxidation, Small 15 (2019), https://doi.org/10.1002/smll.201900153.
[55] L. Zhang, W. Peng, W. Wang, Y. Cao, G. Fan, Y. Huang, M. Qi, A comprehensive review of the electrochemical advanced oxidation processes: detection of free radical, electrode materials and application, J. Environ. Chem. Eng. 12 (2024) 113778, https://doi.org/10.1016/j.jece.2024.113778.
[56] B.P. Chaplin, Critical review of electrochemical advanced oxidation processes for water treatment applications, Environ Sci Process Impacts 16 (2014) 1182–1203, https://doi.org/10.1039/C3EM00679D.
[57] E. Skolotneva, A. Kislyi, A. Klevtsova, D. Clematis, S. Mareev, M. Panizza, Mathematical modeling of the anodic oxidation of organic pollutants: a review, Environ. Chem. Lett. 22 (2024) 1521–1561, https://doi.org/10.1007/s10311-023-01693-0.
[58] A.J. dos Santos, A.S. Fajardo, M.S. Kronka, S. Garcia-Segura, M.R.V. Lanza, Effect of electrochemically-driven technologies on the treatment of endocrine disruptors in synthetic and real urban wastewater, Electrochim. Acta 376 (2021) 138034, https://doi.org/10.1016/j.electacta.2021.138034.
[59] D. Song, B. Qiao, X. Wang, L. Zhao, X. Li, P. Zhang, Y. Yao, H. Chen, L. Zhu, H. Sun, Degradation of perfluorooctanoic acid by chlorine radical triggered electrochemical oxidation system, Environ. Sci. Technol. 57 (2023) 9416–9425, https://doi.org/10.1021/acs.est.3c02025.
[60] S. Yang, S. Fernando, T.M. Holsen, Y. Yang, Inhibition of perchlorate formation during the electrochemical oxidation of perfluoroalkyl acid in groundwater, Environ. Sci. Technol. Lett. 6 (2019) 775–780, https://doi.org/10.1021/acs.estlett.9b00653.
[61] N. Hald, E. Mast, C. Gately, K. Flores, S. Garcia-Segura, Nanointerfacial engineering of a copper-based electrocatalyst for the selective electrogeneration of ammonia from nitrate pollution, ACS Appl. Mater. Interfaces 17 (2025) 57070–57080, https://doi.org/10.1021/acsami.5c13543.
[62] Q. Yue, J. Lin, H. Chen, In situ reactive oxygen species production for in-depth trace organic contaminant remediation in aquatic environment, Environ. Sci. Technol. 60 (2026) 13259–13279, https://doi.org/10.1021/acs.est.5c17411.
[63] A. Serrà, L. Philippe, F. Perreault, S. Garcia-Segura, Photocatalytic treatment of natural waters. Reality or hype? The case of cyanotoxins remediation, Water Res. 188 (2021) 116543, https://doi.org/10.1016/j.watres.2020.116543.
[64] W. Santacruz, J. Faria, R. De Mello, M.V. Boldrin, A. de J. Motheo, Comparative study of MMO and BDD anodes for electrochemical degradation of diuron in methanol medium, Chemosphere 366 (2024) 143517, https://doi.org/10.1016/j.chemosphere.2024.143517.
[65] H. Katsumata, M. Sada, Y. Nakaoka, S. Kaneco, T. Suzuki, K. Ohta, Photocatalytic degradation of diuron in aqueous solution by platinized TiO_2, J. Hazard. Mater. 171 (2009) 1081–1087, https://doi.org/10.1016/j.jhazmat.2009.06.110.
[66] M.C. Edelahi, N. Oturan, M.A. Oturan, Y. Padellec, A. Bermond, K. El Kacemi, Degradation of diuron by the electro-Fenton process, Environ. Chem. Lett. 1 (2003) 233–236, https://doi.org/10.1007/s10311-003-0052-5.
[67] M.A. Oturan, N. Oturan, M.C. Edelahi, F.I. Podvorica, K. El Kacemi, Oxidative degradation of herbicide diuron in aqueous medium by Fenton's reaction based advanced oxidation processes, Chem. Eng. J. 171 (2011) 127–135, https://doi.org/10.1016/j.cej.2011.03.072.
[68] P. Bumroongsakulsawat, W. Khongthon, V. Pavarajarn, Degradation of diuron in water by electrochemical advanced oxidation in a microreactor: effects of anion contamination on degradation and toxicity, J. Environ. Chem. Eng. 8 (2020) 103824, https://doi.org/10.1016/j.jece.2020.103824.
[69] J.A. Silva Moretto, J.P. Rueda Furlan, A.F. Tonelli Fernandes, A. Bauermeister, N. P. Lopes, E.G. Stehling, Alternative biodegradation pathway of the herbicide diuron, Int. Biodeterior. Biodegradation 143 (2019) 104716, https://doi.org/10.1016/j.ibiod.2019.06.004.